ELSEVIER

Surface Science 423 (1999) 303–323

surface science

# Cobalt on rhenium(0001) – an example of thermally activated layer intermixing and surface alloying

M. Parschau, K. Christmann *

*Institut für Physikalische und Theoretische Chemie, Freie Universität Berlin, Takustrasse 3, D-14195Berlin, Germany*

Received 2 September 1998; accepted for publication 27 November 1998

**Abstract**

The growth and morphology of cobalt thin films deposited onto a Re(0001) surface at 300, 400 and 550 K were followed in the coverage range 0 ML $< \Theta <$ 6 ML by combined low-energy electron diffraction (LEED) and scanning tunneling microscopy (STM). The interaction phenomena are complex and depend strongly on temperature. At 300 K, cobalt nucleates homogeneously on terraces and heterogeneously at steps forming dendritic islands. Larger cobalt coverages lead to incomplete layer growth. Interdiffusion and alloying play a minor role only at 300 K, but become dominant for $T > 400$ K in that different $(2 \times 2)$ phases form within the first Re–Co bilayer, one within the rhenium substrate surface, the others within the cobalt islands. The $(2 \times 2)$ phases can be associated with Re/Co surface alloys of different stoichiometry, depending on cobalt coverage. As the cobalt coverages exceed two monolayers (ML), genuine but incomplete cobalt layers grow. Within the third and fourth cobalt layer, periodic triangular features with a lattice constant of $\sim$28 Å appear in STM, followed by a Moiré pattern for $\Theta > 4$ ML. Both structures produce an incomplete $(10 \times 10)$ LEED pattern. After growth of the fifth or sixth layer the lattice misfit is overcome, and cobalt essentially grows layer-by-layer in a pseudo Frank–van der Merwe mechanism, the details being strongly temperature-dependent. 

*Keywords:* Cobalt; Epitaxy; Low energy electron diffraction (LEED); Low index single crystal surfaces; Metal–metal interfaces; Metal–metal magnetic thin film structures; Rhenium; Scanning tunneling microscopy; Single crystal epitaxy; Surface structure, morphology, roughness, and topography

## 1. Introduction

Thin metal films play an increasingly important role in catalysis, materials science, energy technology, physical electronics and magnetism (see, for example, [1,2]). Owing to extensive experimental and theoretical work during the past decades [3–8], the physics of nucleation and growth as well as the equilibrium shape of metallic films grown by heteroepitaxy can be understood fairly well in terms of thermodynamic and kinetic models. An excellent overview has quite recently been given by Brune [9]. However, comparatively little is known about the early stages of boundary interdiffusion leading to the formation of homogeneous alloy phases. Interdiffusion and alloying are especially crucial when bimetallic systems of miscible or chemically similar constituents are used for heteroepitaxy. Accordingly, various more recent studies have focused on this issue. We refer to quantitative low-energy electron diffraction (LEED) work on the Cu/W(100) system by Hu et al. [10] which proved the formation of an ordered Cu/W surface

* Corresponding author. Fax: +49-30-838-4792; e-mail: kchr@chemie.fu-berlin.de.

0039-6028/99/$ – see front matter 
PII: S0039-6028(98)00926-1

alloy and a $c(2\times2)$ vacancy phase, and to a report by Hutt and Bassett on the Ir/Mo(110) system where, likewise, alloy formation took place at elevated temperatures [11]; numerous other bimetallic alloy systems are listed and dealt with in a survey given by Bardi [12]. Recent scanning tunneling microscopy (STM) investigations could, for certain metal-on-metal systems, establish a 'chemical' contrast on the atomic scale and allowed a direct morphological and element-specific analysis of alloy surfaces. We mention STM work by Wouda et al. [13] on Pt–Rh(100) surface alloys and a report by Robert et al. [14] dealing with the Pb/Cu(100) system which likewise allowed a distinction between lead and copper atoms and provided evidence of an ordered PbCu surface alloy. Frequently, STM studies also one allow to monitor preceding processes such as surface site exchange, adatom-induced surface diffusion and step roughening phenomena, illustrative examples being provided by the Rh-on-Ag(100) [15], Rh-on-Au(111) [16], Ir-on-Cu(100) [17], Co-on-Cu(100) [18] or the Fe-on-Cu(100) systems [19].

Although STM provides atomic resolution, imaging of AB alloy surfaces can be difficult because of a chemical-contrast problem between metal atoms A and B. Principally, STM contrast can have two origins. Either the A atoms are definitely located in a different height level than the B atoms, or they are arranged at the same height, but exhibit a different local tunneling probability. Normally, a decision cannot be made without additional experiments, e.g., ion scattering or quantitative LEED measurements. In particular, cobalt atoms dispersed in a matrix of other transition metals (platinum being a suitable example) can exhibit a large chemical contrast [20] and are often almost invisible with STM, as very recent STM, LEED and Auger electron spectroscopy (AES) studies by Gauthier et al. [21] on $Pt_{25}Co_{75}$ alloy surfaces revealed.

In addition to the chemical-contrast problem, it is generally a difficult task to elucidate the various stages of heteroepitactic growth of chemically reactive constituents. It appears a promising route to unravel the associated processes by a combination of element-specific and/or structure-sensitive methods.

We focus here on the Co-on-Re system, because there is a considerable interest in correlating the structure and morphology of thin films of ferromagnetic transition metals with their magnetic properties. This is documented by a vast number of publications dealing with the structural and magnetic properties of iron, cobalt and nickel thin films on non-magnetic metal single-crystal surfaces. Accordingly, we examine the structure of the respective Co–Re bilayer and possible interdiffusion, mixing and alloying processes which can occur at the phase boundary. An early study by Köster and Horn [22] revealed that cobalt and rhenium form, at temperatures well above 1300 K, a continuous series of solid solutions. Therefore, alloy formation must be considered likely if cobalt films on rhenium are annealed at elevated temperatures.

In the past, the (0001) surfaces of the hcp metals ruthenium and rhenium were repeatedly used as substrates for thin film deposition, with a preference for ruthenium because of its well-known catalytic activity [23,24]. From the wealth of studies that were concerned with cobalt heteroepitaxy we consider only a few articles that are more closely related to our own work. We refer to recent STM work by Hwang et al. [25], who investigated the Co/Ru(0001) system, and another STM study on the Ni-on-Re(0001) system by Stindtmann et al. [26]. Of particular interest here are substrates that can alloy with cobalt, and there have been recent reports especially for cobalt deposition on copper single-crystal surfaces, where massive alloying effects were observed. De la Figuera et al. [27] investigated the Co/Cu(111) system, while Li and Tonner studied cobalt films on the Cu(100) surface [28] as did Wuttig et al. [29].

We have deposited cobalt films onto a Re(0001) surface in submonolayer and monolayer concentrations and examined them with regard to nucleation, structure and growth by means of STM and LEED. While a brief summary of our 300 K data was given in a previous publication [30], we report here the extensive body of LEED and STM data obtained in the temperature range from 300 to 550 K. This range is particularly interesting, because simple cobalt island growth prevails at 300 K, but thermally activated diffusion and layer

intermixing phenomena gain importance at elevated temperatures and lead to a fairly complicated scenario of diffusion processes resulting in the final formation of Co–Re surface alloys. Another report that will present combined TDS, XPS and $\Delta\Phi$ work is in preparation and will appear elsewhere [31].

## 2. Experimental

The preparation as well as the morphological characterization of the cobalt films on the Re(0001) substrate was performed in an ultra-high vacuum (UHV) chamber specifically designed to meet the STM in situ requirements and to also allow sample transfer between the STM head and the UHV manipulator. It contained the standard facilities for preparing and maintaining a clean metal surface, to evaporate cobalt thin films and to characterize the structural and chemical properties of the bimetallic systems; among others, a conventional four-grid electron optics (Varian) for LEED and AES and a tunnel microscope (rasterscope 3000, DME). The microscope was operated in the constant-current mode; sample bias voltages between $+1$ mV and $+400$ mV and tunnel currents between 0.1 nA and 2–3 nA were adjusted. By means of a wobble-stick (WA Technology) and a specifically designed tantalum sample holder, transfer of the sample between the manipulator and tunnel microscope was achieved. In order to damp harmful vibrations, the apparatus rested on commercial shock absorbers (Newport). The microscope could be operated at 300 K only. We would like to add that no filtering procedures were employed to improve the quality of the STM images, neither differentiation nor high-pass filtering.

A combined pumping system consisting of a turbomolecular pump and an ion getter pump provided a base pressure of $10^{-10}$ mbar; even during prolonged cobalt deposition from a Knudsen cell the pressure did not exceed the $10^{-9}$ mbar range, whereby the main constituent of the residual gas was nitrogen (formed by decomposition of boron nitride used as an insulator in the Knudsen cell oven). Careful checks with AES and STM did not reveal any hint of nitrogen contamination of the cobalt film, since nitrogen does not adsorb or dissociate under our experimental conditions.

The disk-shaped Re(0001) sample (diameter $\sim 8$ mm, thickness $\sim 1$ mm) was of 5 N purity. After careful mechanical polishing to a mirror-like finish, it was mounted on a high-precision UHV sample manipulator allowing in situ positioning as well as heating by electron bombardment ($T_{max} \approx 2500$ K). Sample temperatures were measured with a Re/WRe thermocouple spot-welded to the sample holder. [A good heat contact was provided by stiff Cu–Be spring clamps which held the sample in place; the (small) temperature difference function $\Delta T(T)$ between the sample and the sample holder had been carefully calibrated by optical pyrometry.]

Cleaning of the surface was achieved by heating for a few minutes in oxygen ($P_{O_2} = 2 \times 10^{-8}$ mbar) at $T = 1100$ K, followed by a 15 min heating to 1500 K in a hydrogen atmosphere ($P_{H_2} \approx 2 \times 10^{-7}$ mbar) and a final flash to $\sim 2300$ K in order to remove residual oxygen. No argon-ion sputtering was employed to avoid damage of the rhenium surface. The cleaning was continued until LEED and AES revealed the complete removal of sulfur, carbon and oxygen impurities.

Evaporation of cobalt was accomplished by a commercial thermal effusion (Knudsen) cell (WA Technology) containing a graphite crucible loaded with ultra-pure (5 N) cobalt wire (Goodfellows) at $T \approx 1500$ K, where the cobalt vapor pressure is high enough to achieve deposition rates of a few monolayers per hour ($\sim 3$ ML h$^{-1}$).

The as-deposited cobalt films were very clean as routinely checked by AES: cobalt coverages could be estimated conveniently from a direct inspection of the 300 K STM images. We define the coverage $\Theta$ (as usual) as the fraction of cobalt atoms and the number of rhenium surface atoms in the unreconstructed (0001) surface; $\Theta_{Co} = 1$ then corresponds to a concentration of $1.515 \times 10^{19}$ m$^{-2}$. At 300 K, both metals crystallize in the hexagonal-close packed (hcp) lattice, the atomic diameter of cobalt being $d_{Co} = 2.507$ Å and that of rhenium being $d_{Re} = 2.7609$ Å [32]. Accordingly, a

rhenium atom is ~10% larger than a cobalt atom, leading to a considerable (negative) lattice misfit, which will induce lattice strain at the interface during heteroepitactic growth.

## 3. Results

This section is organized as follows. In the first part (Section 3.1) we briefly summarize our room-temperature STM and LEED results including the clean Re(0001) surface. In the second part (Section 3.2) the STM and LEED data obtained at higher temperatures will be presented; i.e., at 400 K (Section 3.2.1) and 550 K (Section 3.2.2).

### *3.1. Nucleation and growth of cobalt on Re(0001) at 300 K*

#### *3.1.1. The clean Re(0001) surface*

In a previous publication [30] we showed that the clean Re(0001) surface consists of large homogeneous terraces and steps of predominantly monoatomic height, whereby the steps are usually (but not always) parallel to the three degenerated directions of densely packed rows of rhenium atoms ($[\bar{1}2\bar{1}0]$, $[2\bar{1}\bar{1}0]$ and $[\bar{1}\bar{1}20]$). The terraces are almost free of crystallographic and chemical defects. On the atomic scale, the surfaces are extremely flat with an average corrugation of less than 0.1 Å and exhibit the expected sixfold symmetry. Accordingly, LEED performed with the clean surface revealed the well-known hexagonal pattern with very sharp spots on a low background. No spot splitting could be observed, indicating that the existence of steps is a local phenomenon only and not a characteristic property of the surface (caused, for example, by a systematic misorientation).

#### *3.1.2. Cobalt deposition at 300 K; nucleation and growth behavior*

We vapor-deposited cobalt atoms onto Re(0001) at 300 K and mapped the surface morphology with the tunnel microscope. In order to examine the cobalt nucleation, we intentionally chose a part of the rhenium surface with a high local concentration of smooth monoatomic steps whose distance varied between ~300 and 1000 Å. Our results are summarized in the STM image series of Fig. 1. A large-scale image (area = 3000 Å × 3000 Å) of the Re(0001) surface covered with ~0.15 cobalt monolayers at 300 K is reproduced in Fig. 1a. The rhenium surface exhibits a variety of adjacent terraces separated by monoatomic steps. Many tiny cobalt islands appear on the terraces, and at the ascending steps small dendritic islands expand on adjacent terraces.

For a closer analysis of the island growth we refer to Fig. 1b, which zooms into an area of 500 Å × 500 Å of Fig. 1a. The height profile in the upper right corner reveals that islands both at step edges and on flat terraces are imaged with a somewhat smaller height than the rhenium steps, and the height difference roughly corresponds to the geometrical height difference between the (0001) planes of rhenium (2.23 Å) and cobalt (2.03 Å). This is compatible with islands that consist of one atomic layer only and also confirms that our STM can monitor height differences fairly precisely.

Homogeneous nucleation can be inferred from the very regularly spaced cobalt islands, while heterogeneous nucleation takes place at the step edges. The island density saturates already at a coverage of $\Theta \approx 0.2$; it then amounts to $7 \times 10^{11}$ islands $cm^{-2}$ which corresponds to a mean distance between adjacent islands of ~150 Å and, hence, to an average mean free path of the cobalt atoms on the rhenium surface of this order of magnitude.

In front of the ascending substrate steps one observes a zone in which the cobalt island density is reduced, pointing to a smaller probability for the formation of cobalt nuclei due to trapping of migrating cobalt atoms at the nearby steps. Fig. 1 further illustrates the systematic depletion of cobalt islands in a small stripe on the downhill side next to a step, which allows us to draw conclusions about the lateral diffusion mechanism of the cobalt islands or nuclei.

The smallest islands on the terraces exhibit a compact triangular shape, while larger islands grow to aggregates with strongly frayed edges indicative of dendritic growth; the respective dendritic arms with their width of ca. 20 Å are roughly

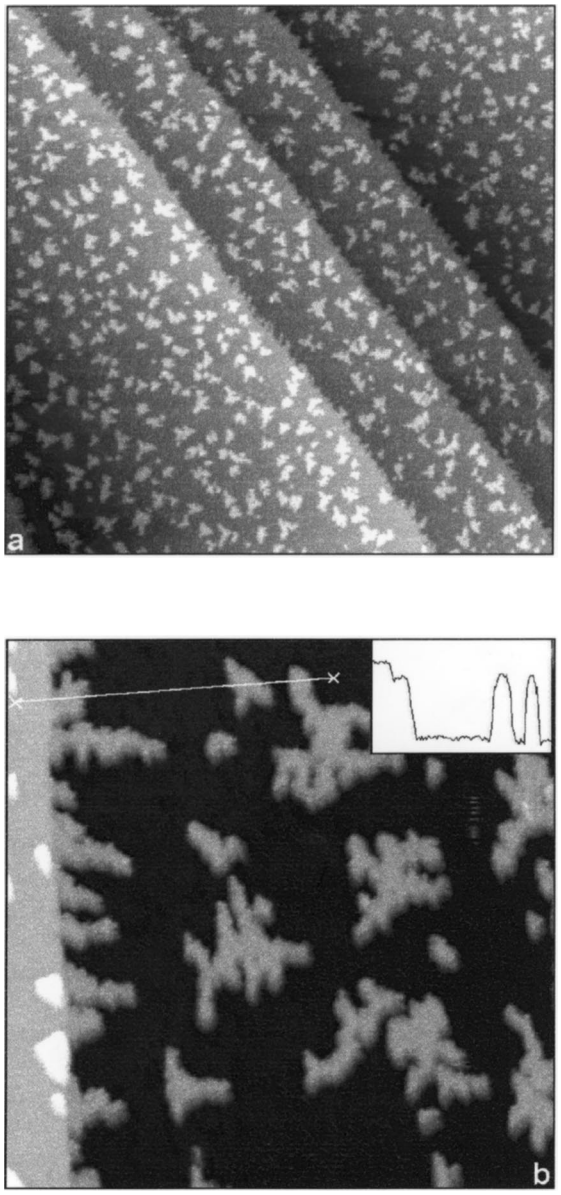


Fig. 1. (a) Large-scale STM image (3000 Å × 3000 Å) of a stepped region of the Re(0001) surface with monoatomic terraces of different widths, after deposition of ~0.15 ML cobalt at 300 K. On the terraces *homogeneous* nucleation takes place, at the step edges *heterogeneous* nucleation. Tunnel conditions: tunnel current, $I_t = 0.10$ nA; bias voltage, $V_t = 30$ mV. (b) STM image of the Re(0001) deposited with cobalt under the same conditions as in Fig. 1a, showing a 500 Å × 500 Å detail next to a step edge on the left side. The dendritic shape of the cobalt islands is clearly recognizable; their monoatomic height follows from the height profile along the white line (inset in the right corner) showing first the height of the upper left rhenium terrace, then the height of the lower rhenium terrace to the right, followed by the heights of two cobalt islands deposited on the lower rhenium terrace ($I_t = 0.22$ nA, $V_t = 41$ mV).

parallel to the three main symmetry directions of the Re(0001) substrate. This type of dendritic growth has been reported frequently in the literature (especially convincingly for the Pt/Pt(111) homoepitactic system [33,34]) and reflects pronounced kinetic limitations in the film growth in that the adatom diffusion along the adatom step edges is strongly restricted. We shall return to this particular point in the discussion (Section 4).

The growth behavior of the cobalt films at larger coverages is illustrated by means of Fig. 2: Figs. 2a and b both depict a representative area of 3000 Å × 3000 Å of cobalt films prepared on a slightly stepped Re(0001) surface at 300 K. Fig. 2a refers to a 0.35 ML film, while the cobalt coverage in Fig. 2b is ~0.8 ML. Since the maximum density of islands is already reached at coverages of ~0.2 ML, no new nuclei are formed at larger coverages but the existing islands merely grow. We draw attention to two features. First, the principal orientation of the fractal arms is rotated by ~60° from terrace to terrace in that the apex of the triangles spanned by the arms either points away from or towards the step, if one proceeds upstairs or downstairs from a given terrace. Furthermore, 'tongues' of cobalt nuclei emerge from the step edges whose direction likewise rotates by ~60° from step edge to step edge. This behavior reflects a slightly different binding situation an adatom encounters when it is added to a step edge in (100) microfacets or in (111) microfacets of the Re(0001) surface as discussed in Section 4.

Increasing cobalt coverages finally cause a loss of the dendritic character of the individual islands, due to the continuous accommodation of cobalt atoms at the existing cobalt aggregates, along with a strongly increased probability of gas-phase cobalt atoms to arrive on an already formed island rather than on the bare Re(0001) surface. Consequently, the individual islands start to coalesce, and second-layer cobalt nuclei begin to form. Exactly this situation is depicted in Fig. 2b, in which the second-layer nuclei appear first as

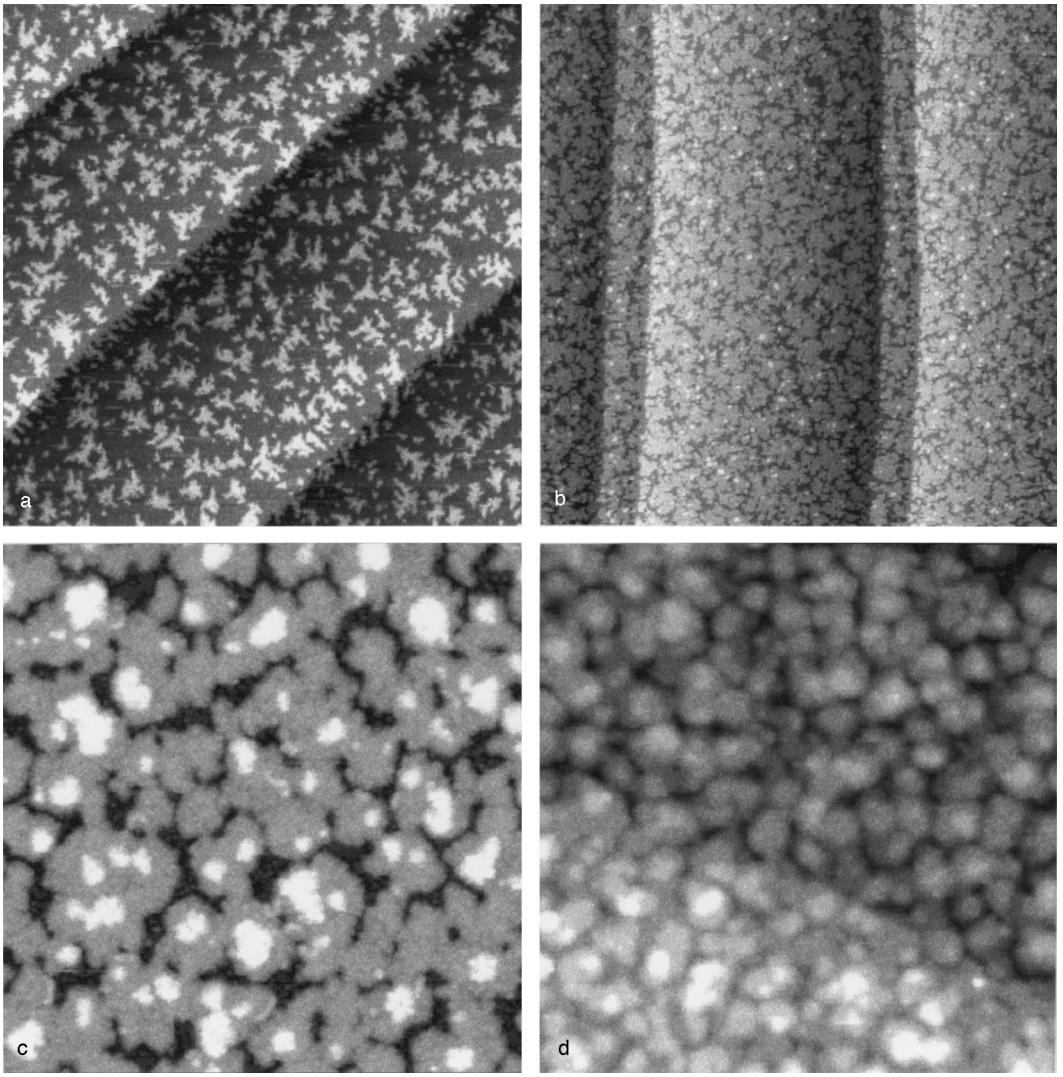


Fig. 2. (a) 3000 Å × 3000 Å detail of a Re(0001) surface with four terraces, separated by monoatomic steps. The cobalt coverage was 0.35 ML at 300 K. Note the relatively high density and the dendritic shape of the cobalt islands as well as the periodic change of the orientation of the 'arms' of the dendritic islands from terrace to terrace. See text for more details ($I_t = 0.40$ nA, $V_t = 90$ mV). (b) Detail (area = 3000 Å × 3000 Å) of a stepped Re(0001) surface covered (at 300 K) with 0.8 ML cobalt and showing the gradual coalescence of islands and the beginning nucleation of cobalt in the second layer; i.e., the sprinkled 'white' points on top of the islands ($I_t = 0.12$ nA, $V_t = 250$ mV). (c) STM image of a 500 Å × 500 Å detail of a 1.9 ML cobalt film deposited at 300 K. Although the second monolayer (irregular gray areas) is not yet completed, 'white' spots indicate growth in the third layer and document the fairly 'open' growth morphology ($I_t = 0.15$ nA, $V_t = 70$ mV). (d) Image of a 900 Å × 900 Å area of a trilayer film including a rhenium step. The dark regions in the upper part represent the first (and practically complete) cobalt monolayer, the grayish islands belong to the second layer, and the light spots on top of these islands are nuclei of the third cobalt layer ($I_t = 0.23$ nA, $V_t = 150$ mV).

sprinkled 'white' spots. The lateral distribution of these spots is fairly irregular and apparently influenced by the dendritic channels and the fairly rough edges of the first-layer islands. We realize that the 'white' cobalt nuclei on top of the first-layer islands are not located somewhere in the center of the large islands, but reside often quite close to the edge. This may be taken as direct

evidence that non-negligible activation energy barriers for surface diffusion exist right at the perimeters of a deposited island; i.e., an active Schwoebel barrier [35] prevents the atoms from 'falling down' into the first layer and filling vacancies there. Even more important may be an attractive potential near the edge of the island which helps to stabilize adatoms on the surface of the island. Altogether, the $\sim 2$ ML cobalt deposit exhibits a fairly 'open' morphology which is characterized by the fact that second-layer nuclei are stable even though the first monolayer is not yet completed (second-layer growth beginning at $\Theta \approx 0.8$ ML).

Still higher coverages lead to an increase in the number of second-layer nuclei and to lateral growth of the individual islands. Note that the cobalt islands in the second layer no longer exhibit the dendritic shape of the first-layer islands; rather their edges are smooth and the islands appear as fairly compact aggregates. In the coverage range after the deposition of almost two nominal cobalt monolayers ($\Theta \approx 2$), nuclei in the third layer begin to form long before the second layer is completed – a situation which is characteristic also for the beginning growth of cobalt atoms in the fourth, fifth, etc. layer. This behavior reflects predominantly the very much restricted lateral diffusivity of the cobalt atoms; in addition, an active Schwoebel barrier may be effective near the edges of the adatom islands. Consequently, the room-temperature growth of cobalt thin films on a clean Re(0001) substrate is characterized by incomplete layer growth (pseudo Frank–van der Merwe type) resulting in relatively rough films, as proved by Fig. 2c showing a $500\ \text{Å} \times 500\ \text{Å}$ detail of an almost completed bilayer cobalt film ($\Theta = 1.9$ ML) and Fig. 2d which displays a $900\ \text{Å} \times 900\ \text{Å}$ area of a trilayer film including a rhenium step. The dark areas in the upper half represent the first (and practically complete) cobalt monolayer, the grayish islands belong to the second layer, and the light spots on top of these islands are nuclei of the third cobalt layer.

LEED investigations carried out with cobalt films in the coverage range $1\ \text{ML} < \Theta < 3\ \text{ML}$ clearly reveal that films grown on Re(0001) at 300 K can exhibit considerable long-range order. While no LEED superstructure appears up to cobalt coverages of $\sim 1.5$ ML, the deposition of $\sim 2$ ML causes 'extra' spots which lead to an apparent doubling of the hexagonal Re(1×1) LEED pattern: the hexagonal rhenium pattern is surrounded by a well-aligned, somewhat larger hexagon with slightly more diffuse spots. A typical pattern is reproduced in Fig. 3 for a 2.4 ML cobalt film. It indicates heteroepitactic cobalt growth in which the individual crystallites possess their own characteristic lattice constant, but are aligned in such a way that their densely packed rows of atoms are parallel to the respective symmetry directions of the rhenium substrate. A comparison of the reciprocal vectors of the rhenium and the cobalt lattice can easily be performed using the spot-splitting in the LEED pattern and yields, with $a^*_{\text{Re}} = 0.362\ \text{Å}^{-1}$, a real-space lattice vector for cobalt of $a_{\text{Co}} \approx 2.5$ Å. This number is actually very close to the literature value for bulk hcp cobalt and demonstrates that this element can grow with its own lattice parameters already after deposition of only two or three layers, despite the considerable lattice misfit of $-10\%$. For a determination of the stacking sequence (hcp versus fcc),

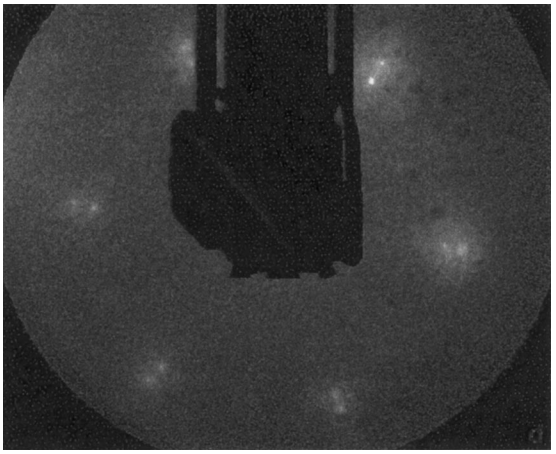

Fig. 3. LEED pattern obtained from a Re(0001) surface after deposition of 2.4 ML cobalt at 300 K indicating heteroepitactic growth (electron energy, $E_p = 112$ eV). The characteristic hexagonal rhenium spots are superimposed by a well-aligned, somewhat larger hexagon with slightly more diffuse spots. The spot doubling allows an estimation of the lattice constant of the cobalt film, in comparison with the rhenium substrate, see text for more details.

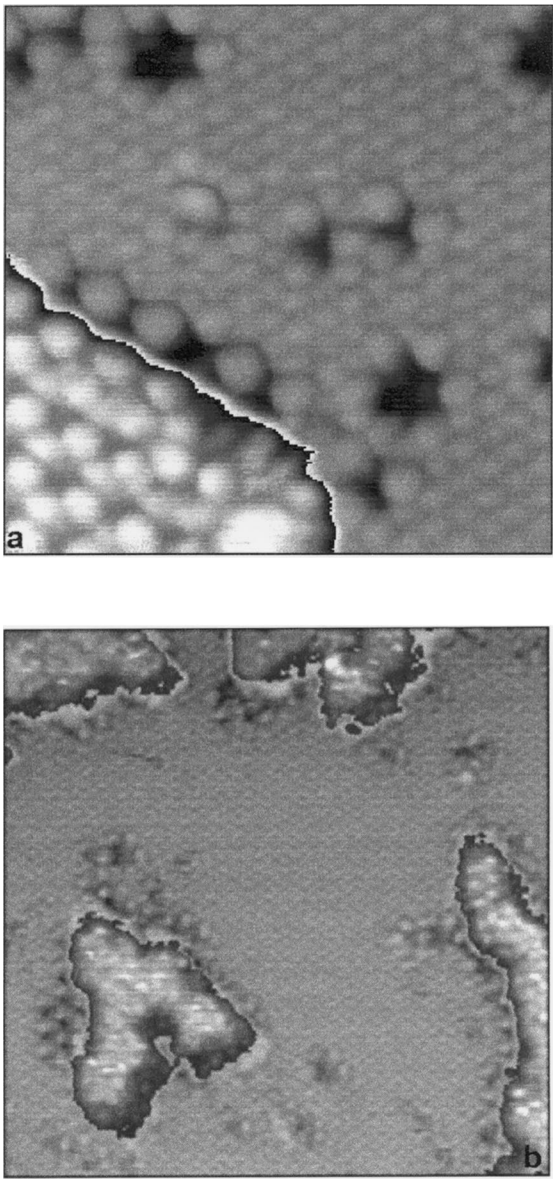


Fig. 4. (a) STM image taken from ~0.3 ML cobalt film with atomic resolution (area = 50 Å × 50 Å) showing the edge and the 'rhenium vicinity' of a small cobalt island. The cobalt atoms appear bright, the rhenium atoms dark. Within the island, the cobalt atoms possess some (hexagonal) short-range order only. Note the cobalt-induced 'perturbations' of the regular hexagonal morphology of the Re(0001) surface, especially at the borderline to the island. They consist of triangular- and hexagonal-shaped 'holes' with somewhat 'inflated' neighbor atoms (rhenium) indicating pronounced changes of the local electronic charge distribution near the perturbations ($I_t$ = 0.75 nA, $V_t$ = 8 mV). (b) STM image presenting an area of 150 Å × 150 Å of the rhenium surface covered (at 300 K) with sprinkled cobalt islands to a total coverage of $\Theta \approx 0.15$. While most of the uncovered rhenium area is still (1 × 1)-oriented, some patches exhibit a clear (2 × 2) superstructure. The (2 × 2) pattern seems to contain periodic 'vacancies' in the rhenium surface, but a closer consideration reveals that the vacancies are actually filled by cobalt atoms that cannot be imaged by STM due to a strong chemical contrast ($I_t$ = 0.98 nA, $V_t$ = 5 mV).

a careful dynamical LEED analysis would be required that has not yet been performed.

### *3.1.3. The onset of rhenium restructuring and ordering within the first bilayer at 300 K*

A closer inspection of the STM features reveals that the 'simple' growth of cobalt islands on top of the rhenium surface described above represents half the truth only: STM images taken from ~0.3 ML cobalt films with atomic resolution are displayed in Fig. 4 and allow one to distinguish individual atoms of both the substrate and the cobalt film. A particularly revealing detail (area = 50 Å × 50 Å) is shown in Fig. 4a, namely the edge and the 'rhenium vicinity' of a small cobalt island (in this image, the cobalt atoms appear bright and the rhenium atoms dark). Within this island, the cobalt atoms possess (hexagonal) short-range order only, in agreement with parallel LEED observations. These showed just an increase in the diffuse background diffraction intensity, but no cobalt-induced 'extra' spots nor a change of the intensity–voltage ($I$–$V$) behavior of the Re(1 × 1) LEED beams, thus ruling out pseudomorphic growth of cobalt under these conditions.

Another feature of Fig. 4a deserves attention, because it is crucial for understanding the processes which take place at elevated temperatures (cf. Section 3.2): while the clean Re(0001) surface is, over large distances, almost free of point defects, Fig. 4a exhibits such defects in the rhenium surface which appear as 'dark' holes or apparent 'vacancies' especially in the vicinity of the cobalt island. In some cases, these defects even exhibit the beginning of long-range order as displayed in Fig. 4b; this presents a somewhat larger area (150 Å × 150 Å) of the rhenium surface covered with sprinkled cobalt islands to a total coverage

of ~0.15. While most of the uncovered rhenium area is still (1×1)-oriented, some patches exhibit a clear (2×2) superstructure. Finally, we note that a (2×2) structure also begins to develop inside the cobalt islands.

### 3.2. Deposition of cobalt onto Re(0001) at elevated temperatures (T>300 K)

We performed cobalt deposition and annealing experiments at 400 and 550 K, respectively. Although many of the morphological features of the Co/Re(0001) system can be observed in a similar manner at both temperatures, there are nevertheless some specific processes and phenomena that are different, and it is perhaps useful to devote a separate section to each deposition/annealing temperature.

#### 3.2.1. Interaction between cobalt and rhenium at 400 K

*3.2.1.1. LEED.* In contrast to the cobalt deposition at 300 K, where LEED only showed an increase of the diffuse intensity and finally the occurrence of a hexagonal epitactic cobalt phase, exposure of the Re(0001) surface to cobalt vapor at $T=400$ K causes a clear (2×2) LEED pattern which is reproduced in Fig. 5a. It appears for the first time after deposition of ~ 0.3 ML, and the intensity maximum of the fractional-order beams is reached and passed around $\Theta_{Co}\approx 1$. The intensity of the fractional-order LEED spots is somewhat lower than the integer-order rhenium beams; also their sharpness is first not as pronounced as the Re(1×1) LEED spots. [However, both sharpness and intensity of the cobalt-induced LEED beams increase markedly upon a short annealing to 550 K, indicating an improvement of the long-range order within the cobalt-induced (2×2) phase(s).]

As more cobalt is deposited at 400 K, the (2×2) LEED pattern is retained, until after deposition of two complete cobalt layers the same hexagonal cobalt pattern also becomes visible and is superimposed on the (2×2) structure which was observed already at room temperature. The respective LEED pattern is reproduced in Fig. 5b. Obviously, genuine cobalt crystallites of hexagonal orientation grow on top of the (2×2) phase in a very similar manner as described above for 300 K deposition. Quite remarkably, however, cobalt deposition of ca. 3 ML produces another, more complicated, LEED pattern (shown in Fig. 5c) which we identify as an (incomplete) (10×10) structure. In this pattern only the first, second and (quite weak) third-order beams are visible, and the former (2×2) structure has practically disappeared. The occurrence of a (10×10) pattern suggests a phase in real-space which has a periodicity of 10 times the Re–Re distance; i.e., approximately 28 Å. The (10×10) structure is only transient; as the cobalt deposition is continued to beyond 4 ML, it disappears again, and we are finally left with the clear (1×1) LEED pattern of hexagonal symmetry caused by the well-oriented (111) epitactic cobalt overlayer.

We recall that it had been impossible to generate an intense (2×2) or the (10×10) phase at room temperature. However, we succeeded in obtaining these phases with a comparable crystallographic quality simply by heating and annealing the 300 K cobalt deposit for only some minutes to 400 K, as shown in Fig. 5d. Since it is well-known that long-range ordering of disordered films (by lateral diffusion) can hardly be accomplished simply by heating [36], we argue that an *interfacial reaction* may be responsible for the observed effects as pointed out in Section 4.

*3.2.1.2. STM.* At 400 K, the mean distance between adjacent cobalt islands, as well as the width of the depletion zone in front of the ascending rhenium steps, increase. In addition, deposition of 0.1 ML of cobalt at 400 K induces peculiar morphological changes of both the rhenium surface and the cobalt islands as shown in Fig. 6a. First of all, the islands have no longer a dendritic shape, but the surface becomes sparsely covered with a few larger and much more compact two-dimensional cobalt islands of relatively regular triangular shape. What we saw already at room temperature, namely a beginning of restructuring of both the rhenium and the cobalt surface leading to (2×2) patches in the direct vicinity of a cobalt island, is now greatly enhanced. First, the localized

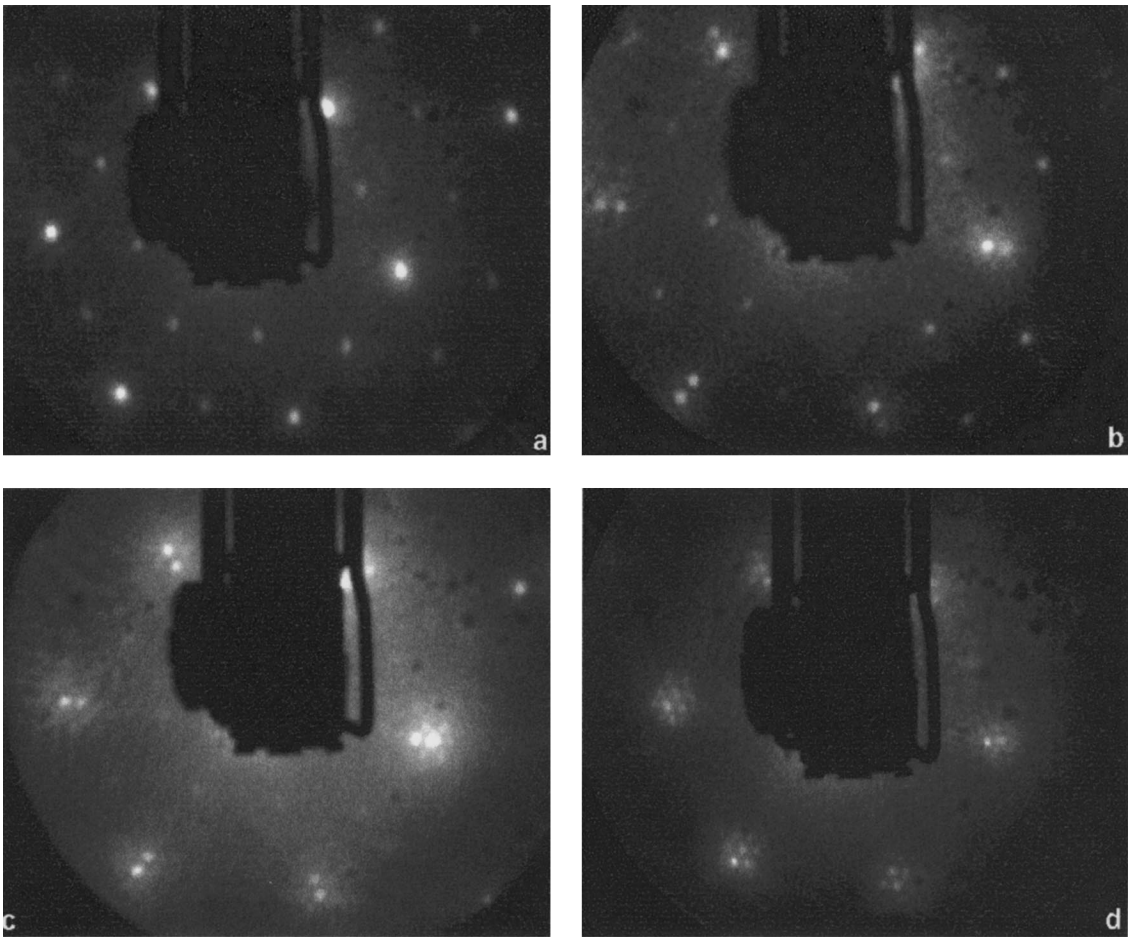


Fig. 5. LEED patterns of a cobalt-covered Re(0001) surface after deposition at 400 K, displaying various cobalt coverages. (a) $\Theta_{Co}=1$ ML: a clear $(2\times2)$ superstructure (weak spots) is superimposed to the Re$(1\times1)$ pattern (bright LEED spots). The electron energy was $E_p=98$ eV. (b) Coexistence of the $(2\times2)$ LEED structure and the hexagonal $(1\times1)$ LEED pattern of the epitactic cobalt islands (outer spots of the doublets), after deposition of 1.8 ML cobalt. The electron energy was $E_p=88$ eV. (c) $(10\times10)$ LEED structure obtained after deposition of $\sim3.2$ ML at 400 K. The spots of the former $(2\times2)$ structure are still visible, although only very weakly (electron energy $E_p=108$ eV). (d) $(10\times10)$ LEED pattern after short annealing of a 3.2 ML cobalt film at 550 K originally deposited at 300 K. Note the absence of the $(2\times2)$ superstructure under these conditions (electron energy $E_p=115$ eV).

perturbations spread across the entire surface, resulting in a large number of point defects (holes, vacancies) everywhere on the uncovered parts of the rhenium surface. Second, increasing surface areas, even far away from the cobalt-containing islands, transform to the Re$(2\times2)$ 'vacancy' structure. Furthermore, the cobalt-containing triangular islands on top of the rhenium surface themselves rearrange to a pronounced $(2\times2)$ structure (average diameter of the reconstructed patches at least 50 Å), whereby the orientations of the individual patches become increasingly correlated. This is illustrated in Fig. 6b. However, apart from the common $(2\times2)$ periodicity, it is apparent from the STM results presented in the following that this phase differs considerably from the 'vacancy' structure formed on the bare rhenium surface. [Any difference in the unit meshes of the $(2\times2)$ structures could, of course, not be deduced from the mere inspection of the $(2\times2)$ LEED pattern.]

Next, we undertake the attempt to analyze the

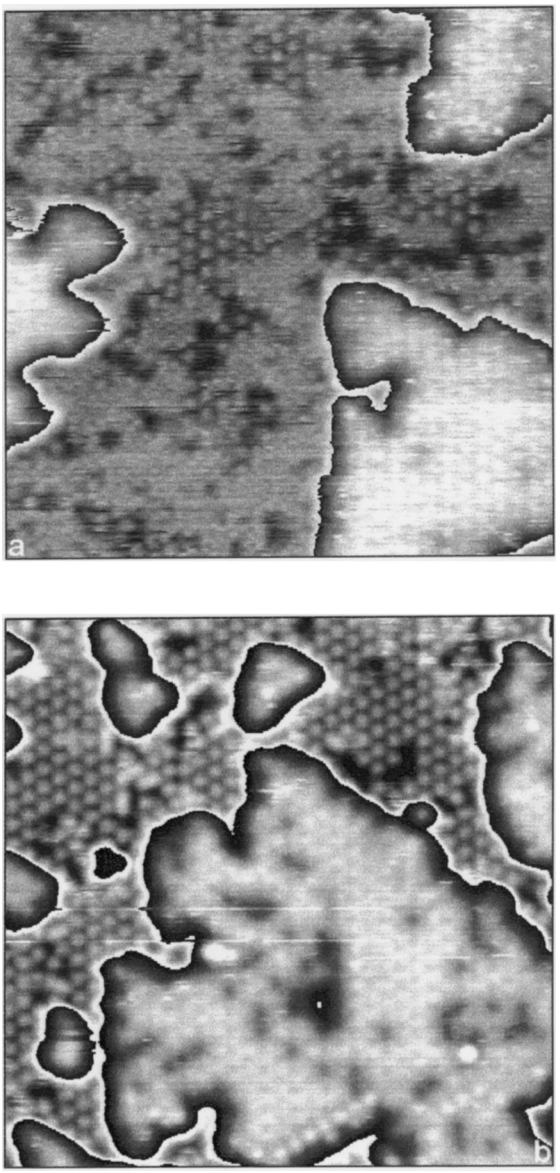


Fig. 6. Morphological changes occurring in the rhenium surface after deposition of submonolayer amounts of cobalt at 400 K. (a) 150 Å × 150 Å detail showing the beginning of $(2\times2)$ restructuring of the Re(0001) surface between cobalt islands and the loss of the dendritic shape of the islands (which are represented by the light triangular-shaped areas). The cobalt coverage is 0.4 ML ($I_t=0.45$ nA, $V_t=1$ mV). (b) STM image (160 Å × 160 Å) of a ~0.6 ML cobalt film deposited at 400 K showing a large triangular-shaped cobalt island with fringed edges in a 'sea' of $(2\times2)$ reconstructed rhenium. The island itself also exhibits a $(2\times2)$ structure, which differs from the one of the rhenium surface ($I_t=0.31$ nA, $V_t=5$ mV).

local structure of the two $(2\times2)$ phases formed on the cobalt-free parts of the rhenium surface and 'inside' the 'cobalt' islands, respectively, by atomically resolved STM observations. In order to learn more about the details of the local structure, we zoomed into the two $(2\times2)$ phases by choosing very low tunnel currents (<1 nA) and bias voltages. Fig. 7a shows a largely magnified STM image (area = 52 Å × 52 Å) of a rhenium surface which was covered by ~0.4 ML cobalt at 400 K. It proves coexistence of the $(2\times2)$ 'vacancy' phase and the 'regularly' structured hexagonal rhenium surface, whereby the islands of both phases exhibit a triangular shape. The same gray scales of the atoms in the $(1\times1)$ and $(2\times2)$ phases clearly underline that these atoms reside approximately at the same height level, but it is not possible to further magnify the 'vacancy' structure and to answer the question whether or not additional cobalt atoms are incorporated in this phase.

However, a closer inspection of Fig. 7a reveals two kinds of 'vacancies': one kind (outside the vacancy phase) about 1 Å deep, and the other kind (inside the 'vacancy' phase) only about 0.5 Å deep. This fact could indicate that the surprisingly 'open' structure of the rhenium surface in the $(2\times2)$ phase is stabilized by cobalt atoms that are incorporated in the rhenium surface and/or in the second layer underneath the rhenium surface, but this remains somewhat speculative. These uncertainties make us hesitate to argue too much about possible stoichiometries of this surface alloy (which would be $ReCo_3$, if every 'dark hole' would represent a cobalt atom).

In order to tackle the next problem of the locations in which the replaced rhenium atoms become accommodated, we recall our observation whereafter another $(2\times2)$ phase is formed inside the cobalt-containing islands. This phase can also be directly seen in STM images with atomic resolution, cf. Fig. 7b. This image, showing a 50 Å × 50 Å detail of a ~0.7 ML film, exhibits a pronounced $(2\times2)$ structure; its lattice parameter is likewise exactly twice the Re$(1\times1)$ lattice constant (as in the 'vacancy' structure). We associate the large (light) atoms with rhenium and the small (dark) atoms in their direct vicinity with cobalt

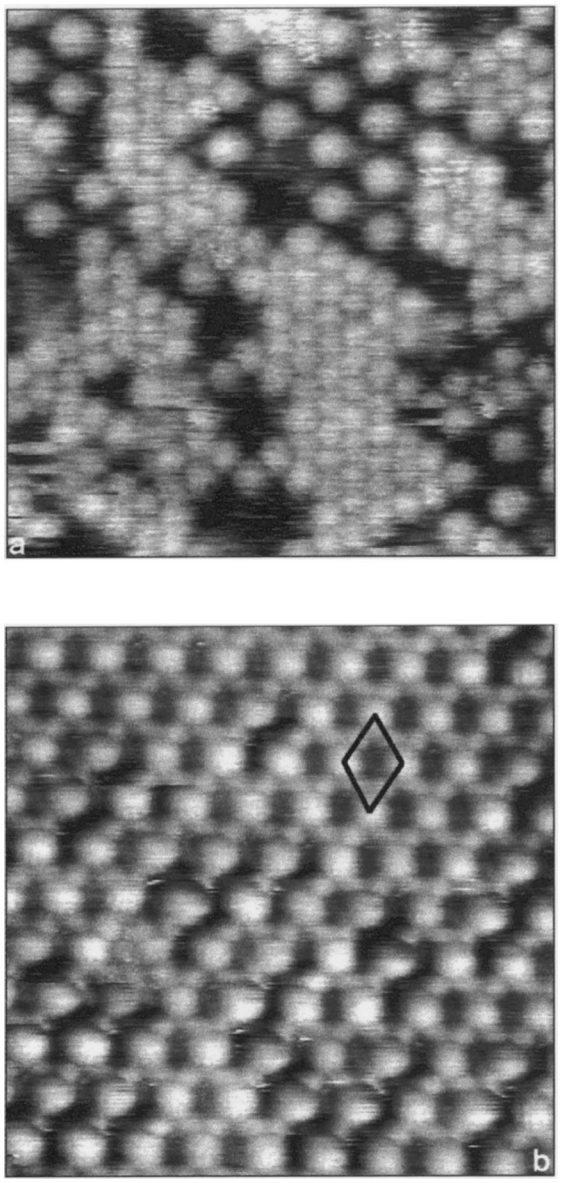


Fig. 7. (a) Largely magnified STM image (area = 52 Å × 52 Å) of a rhenium surface covered with ~0.4 ML cobalt at 400 K, proving the coexistence of the (2 × 2) 'vacancy' phase and the 'regularly' (1 × 1) structured hexagonal rhenium surface. The atoms inside the respective triangular islands of both phases are on the same height level. There is strong evidence that the 'holes' of the 'vacancy' phase actually represent (invisible) cobalt atoms. Then this phase represents a surface alloy with composition $ReCo_3$ ($I_t$ = 0.82 nA, $V_t$ = 1 mV). See text for the details. (b) Atomically resolved STM image of the (2 × 2) phase inside the cobalt islands showing a 50 Å × 50 Å detail of a ~0.7 ML cobalt film. The lattice parameter is twice that of the Re(1 × 1) lattice constant (as in the 'vacancy' structure). The larger (light) atoms are associated with rhenium and the smaller (dark) neighbor atoms with cobalt atoms. Note that the rhenium atoms are surrounded by four cobalt atoms, suggesting a regular surface alloy of stoichiometry $ReCo_2$ ($I_t$ = 0.3 nA, $V_t$ = 1 mV).

atoms, see below. The dark atoms are arranged in chains along one of the high-symmetry directions of the Re(0001) surface; locally, always four of them surround a given rhenium atom, and we therefore interpret this (2 × 2) phase as a Re–Co surface alloy with the stoichiometry $ReCo_2$. However, in this surface alloy we face again the problem of chemical contrast versus perpendicular displacement of the constituent atoms. If we assume zero chemical contrast, the STM image of Fig. 7b would suggest a height difference of ~0.2 Å between the rhenium and the cobalt atoms which (presumably entirely accidentally) corresponds exactly to the geometric height difference between 'hard' spheres of cobalt and rhenium atoms arranged in the same lattice plane. That the imaging contrast plays nevertheless a decisive role here can be inferred from the largely different diameters of the 'light' and 'dark' atoms which deviate strongly from their geometrical values ($d_{Co}$ = 2.50 Å; $d_{Re}$ = 2.76 Å): in Fig. 7b the 'light' atoms are about twice as big as the 'dark' atoms. The only criterion for identifying the kind of atom must then be based on the lateral distances of the atoms. A detailed inspection of the distances between the 'dark' atoms in the $[\bar{1}2\bar{1}0]$ direction reveals two different distances to the nearest neighbors, one being 2.5(±0.1) Å, the other 2.9(±0.1) Å. The first value is markedly smaller than the Re–Re distance (of 2.76 Å), but very much resembles the Co–Co distance in the (0001) plane. Since a compression of rhenium atoms of this magnitude is certainly unrealistic, we are quite sure that the small 'dark' atoms actually represent cobalt. This assignment solves the aforementioned problem of the final location of those rhenium atoms which became removed from the Re(1 × 1) surface during formation of the (2 × 2) 'vacancy' phase. The presence of a stoichiometric surface alloy also in the cobalt islands strongly suggests that these rhenium atoms are able to diffuse to

the borderlines of the cobalt islands where they become incorporated or better dissolved to form the periodic $(2\times2)$ alloy phase $ReCo_2$.

### 3.2.2. Interaction between cobalt and rhenium at 550 K

*3.2.2.1. LEED.* Compared with the situation at 400 K described above, the LEED features do not principally change. We still observe a clear $(2\times2)$ pattern in the submonolayer range, followed by the hexagonal 'epitactic' pattern after deposition of $\sim$1.5 ML and a pronounced $(10\times10)$ structure between $\sim$2 and 4–5 ML whose order is significantly better than the one observed at 400 K. Finally, after deposition of more than five layers, Co(111) spots dominate the LEED pattern, indicating clear epitactic growth of hexagonal cobalt crystallites.

*3.2.2.2. STM.* The STM images taken from the 550 K films reveal substantial morphological changes as compared with the 400 K situation. These can best be visualized by a comparison of two images (300 Å $\times$ 300 Å) of practically the same part of the cobalt-covered rhenium surface, cf. Figs. 8a and b. The upper image (Fig. 8a) shows a cobalt film with $\Theta=0.75$ at 400 K, the lower image (Fig. 8b) a film with $\Theta=0.55$ at 550 K. The somewhat darker areas represent the Re(0001) surface (of course, largely altered by incorporated cobalt atoms), the triangular light-gray patches the cobalt islands, also modified by incorporated rhenium atoms. In the 400 K film, the $(2\times2)$ 'vacancy' phase persists on the Re(0001) surface as demonstrated by the patch in the central part of Fig. 8a. Only locally, rows or chains with apparently missing atoms appear, mostly right at the borderlines of the islands. The dark 'holes' represent the already mentioned 'vacancies' of the Re$(2\times2)$ surface structure, while the respective 'holes' in the cobalt-containing islands are characteristic of the $ReCo_2$ surface alloy. Fig. 8b illustrates the situation after cobalt deposition of 0.55 ML, and apparently the formation of chain-like arrays of atoms sets in at considerably smaller coverages. At $\Theta=0.55$, almost the entire surface consists of this chain structure which is particularly

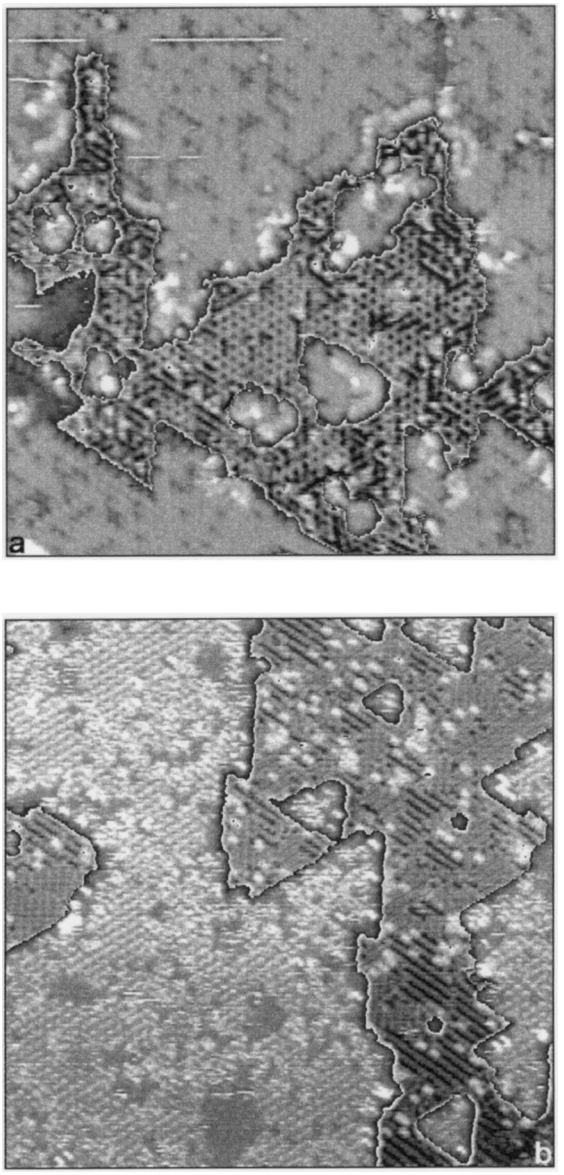


Fig. 8. Two tunnel images showing the influence of temperature on the cobalt-induced surface restructuring. The darker parts of both 300 Å $\times$ 300 Å large areas represent the reconstructed rhenium surface, the lighter grayish areas the (likewise restructured) cobalt islands. In detail: (a) Re(0001) surface after deposition of 0.75 ML cobalt at 400 K, showing the $(2\times2)$ 'vacancy' ($ReCo_3$ alloy) phase in the rhenium surface and the (different) surface alloy $(2\times2)$ phase ($ReCo_2$) ($I_t=0.2$ nA, $V_t=32$ mV). (b) Re(0001) surface after deposition of 0.55 ML cobalt at 550 K. While a $(2\times2)$ phase still dominates in the cobalt islands, the rhenium part of the surface undergoes heavy reconstruction: among others, double rows are formed which are clearly recognizable in the lower part of the image ($I_t=0.1$ nA, $V_t=22$ mV).

well developed in the lower right corner of Fig. 8b. This chain structure not only consists of missing rows of atoms, but it also exhibits double rows made of atoms with slightly different chemical contrast. This can be seen from STM images with atomic resolution, cf. Fig. 9. Fig. 9a shows a 120 Å × 120 Å detail of a 0.55 ML cobalt film at 550 K. In the $(\bar{1}2\bar{1}0)$ direction several rows of atoms are missing, while in the other two symmetry-equivalent directions double rows can be distinguished. Fig. 9b reveals small, but distinct, contrast differences in these double rows which we associate again with cobalt and rhenium atoms located in the same lattice plane, but exhibiting different chemical contrast. Due to the somewhat smaller diameter of a cobalt atom the double rows can shrink somewhat, giving rise to depression lines which are imaged as dark lines next to the double rows. The row entities can be considered as a Co/Re alloy with equal numbers of cobalt and rhenium atoms; they are not only geometrically different from the $(2\times2)$ phases, but likely also with respect to their chemical composition. At any rate, the features of Figs. 8 and 9 seem to indicate that a higher interaction temperature favors a better intermixing of the rhenium and cobalt atoms at the interface.

In addition to the morphological changes occurring on the rhenium surface, the structure inside the CoRe alloy islands is also significantly altered as demonstrated by Fig. 10 which shows an atomically resolved 33 Å × 33 Å detail of a ~0.4 ML cobalt film prepared at 550 K. Again, we observe a $(2\times2)$ phase which is, however, different from the $(2\times2)$ alloy $ReCo_2$ formed at 400 K. A close look at Fig. 10 reveals that an additional cobalt atom is included in the $(2\times2)$ unit mesh, since each large (light) rhenium surface atom is symmetrically surrounded by three cobalt atoms (appearing as smaller and darker spheres in Fig. 10). We may thus conclude that the formation of a surface alloy with composition $ReCo_3$ is favored at elevated temperatures.

Interesting conclusions about the heteroepitactic growth of cobalt on Re(0001) can be drawn from experiments in which the amount of cobalt deposited at 550 K is further increased. Starting point for these deposition experiments are the two

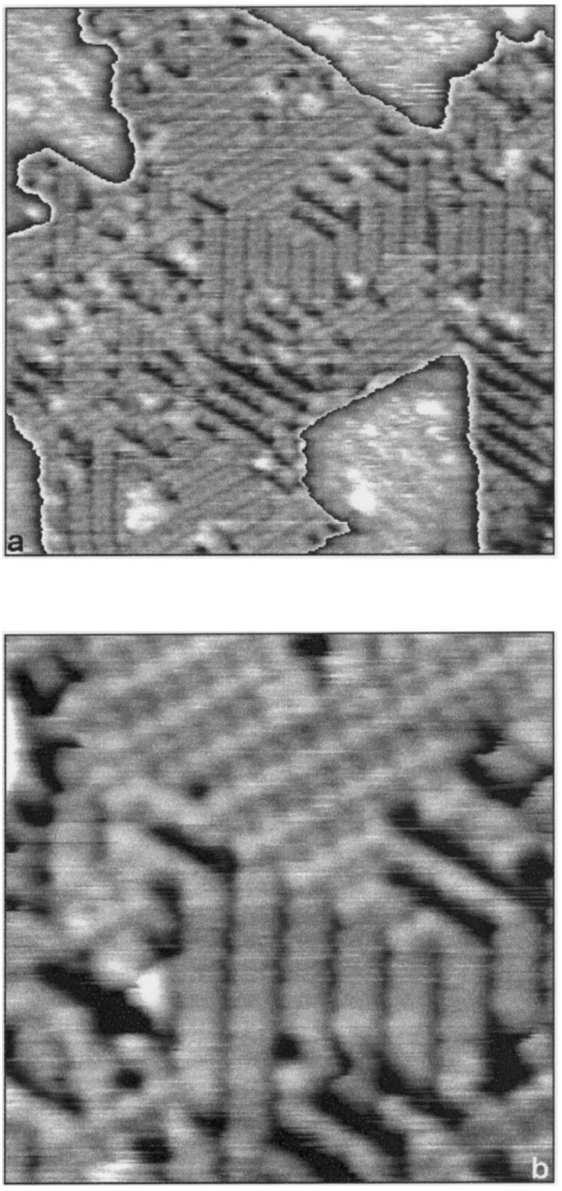


Fig. 9. Surface alloy phases formed after deposition of ~0.55 cobalt coverage equivalents at 550 K, monitored by STM. (a) Rhenium part of the surface (120 Å × 120 Å) that has undergone restructuring due to the formation of CoRe double rows ($I_t$ = 0.15 nA, $V_t$ = 16 mV). (b) Same part of the surface in a larger magnification (50 Å × 50 Å) showing the chemical contrast between the (lighter) rhenium and the (darker) cobalt atoms especially in the upper part of the figure ($I_t$ = 0.15 nA, $V_t$ = 5 mV).

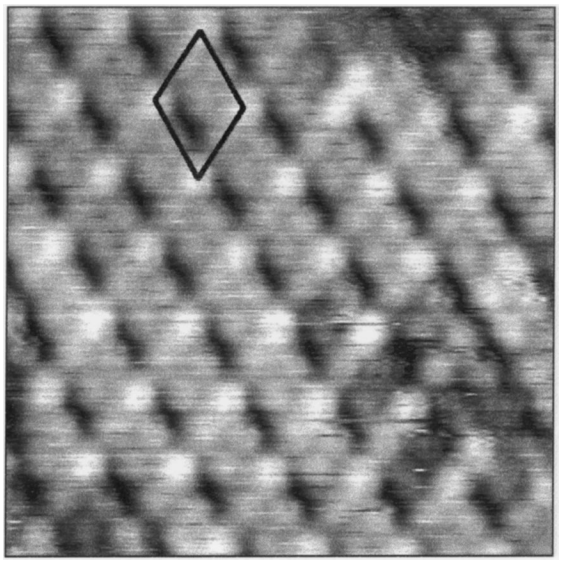

Fig. 10. Atomically resolved 33 Å × 33 Å detail of a ~0.4 ML cobalt film prepared at 550 K. The image has been taken from the interior of a restructured cobalt island and shows that the (2 × 2) phase is not identical to the $ReCo_2$ phase formed at 400 K, but contains an additional cobalt atom in the unit mesh. Each large (light) rhenium surface atom is symmetrically surrounded by three cobalt atoms (which are imaged as smaller and darker spheres in the figure) ($I_t$ = 2.0 nA, $V_t$ = 5 mV).

(2 × 2) surface alloys which occur in the Re/Co bilayer right at the interface. Deposition of two or three cobalt layers on top of this open and partially reconstructed bilayer leads to the formation of a fairly regular network of small equilateral triangles, as reproduced in Fig. 11a. The triangles have two slightly different sizes, one with side length of ~21(±2) Å and imaged in a grayish contrast, the other one with a length of ~27(±2) Å appearing lighter. The apparent height difference between these triangle structures (which are rotated by 180° against each other) is approximately 0.3 Å. These structural features remind us of typical misfit dislocation domain structures previously reported, e.g., for silver on Pt(111) [40] or silver on Re(0001) [36], in which crystallites of adatoms grow with their own lattice constant on top of a host substrate. However, this phase is followed by another, final phase if the deposition at 550 K is extended to the fourth, fifth or sixth cobalt layer. As documented in the STM image of Fig. 11b, this phase (which is difficult to observe) exhibits a markedly smaller corrugation and has about the same periodicity of 27 Å as the triangular structure of the second and third layers. Both structures are probably responsible for the (10 × 10) LEED pattern described before. As will be pointed out in greater detail in the discussion section, we associate this final structure with a Moiré pattern formed by superposition of (possibly rotated) hexagonal lattices with slightly different lattice parameter.

## 4. Discussion

One essential result of our work is that the interaction of cobalt atoms with the hexagonal Re(0001) surface is strongly temperature-dependent. At 300 K the growth of genuine cobalt islands is the dominating process, and Co–Re site exchange and alloying or interdiffusion phenomena still play a minor role. However, at even slightly higher temperatures these latter processes take over, although they remain always restricted to the first Re/Co bilayer.

### *4.1. Nucleation and growth of cobalt on Re(0001)*

The system Co/Re(0001) is a clear example of homogeneous nucleation; only at the edges of substrate steps and at defect sites also, heterogeneous processes occur. The observed island density of $7 \times 10^{11}$ cm$^{-2}$ is relatively high compared with densities reported for other heteroepitactic systems, the reason likely being a restricted lateral mobility of cobalt on Re(0001). For the noble metals gold and copper deposited at 300 K and with comparable rates (0.2–0.4 ML min$^{-1}$) on the similar Ru(0001) surface, maximum island densities of $3 \times 10^8$ cm$^{-2}$ and $5 \times 10^9$ cm$^{-2}$ were obtained, respectively, while the deposition of cobalt on Ru(0001) revealed $3 \times 10^{10}$ cm$^{-2}$ [25,37]. With the homoepitactic systems Ni/Ni(100) and Au/Au(100) comparable island densities were reported, namely $2 \times 10^{12}$ cm$^{-2}$ [38] and $3 \times 10^{11}$ cm$^{-2}$ [37], the reason being the considerably higher diffusion activation barrier on the more open (100) surfaces than on the close-packed hexagonal (0001) faces [39]. The relatively large activation barrier for surface diffusion of cobalt

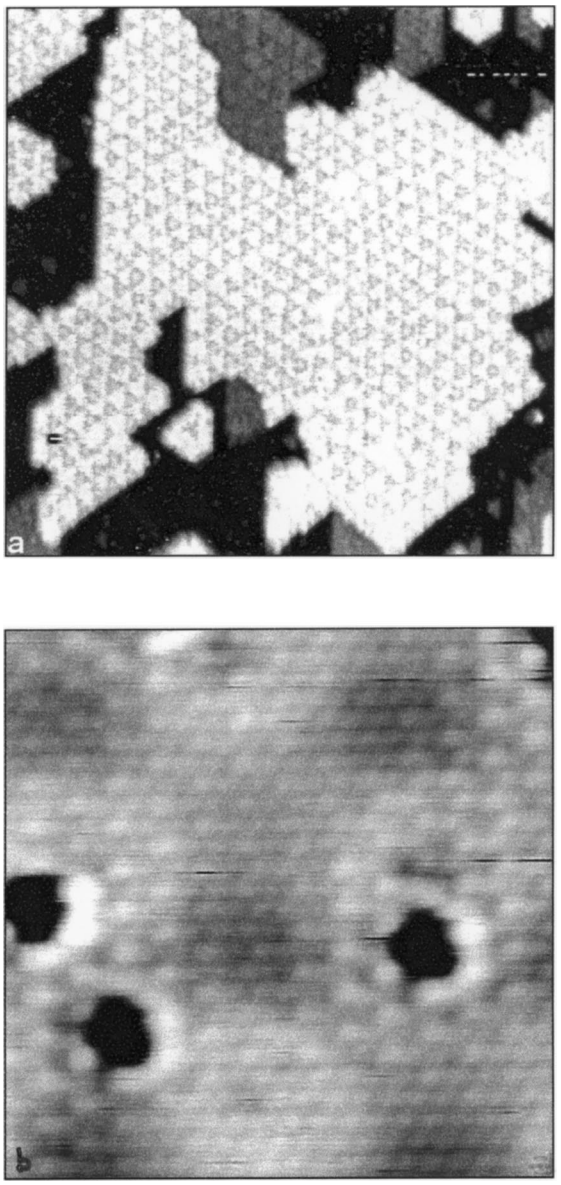


Fig. 11. STM images illustrating the growth behavior of cobalt films on Re(0001) at 550 K in the multilayer regime. For the coverages shown, periodic structures with a period length of $\sim 28$ Å are formed which are responsible for the $(10 \times 10)$ LEED pattern reproduced in Fig. 5d. (a) Deposition of two or three cobalt layers on the reconstructed Re/Co bilayer reveals a network of equilateral triangles which we associate with regular misfit dislocation domains. The triangles have two slightly different sizes, one with side length of $\sim 21(\pm 2)$ Å and imaged in a grayish contrast, the other one with a length of $\sim 27(\pm 2)$ Å appearing lighter (800 Å × 800 Å; $I_t = 0.1$ nA, $V_t = 100$ mV). (b) Moiré pattern observed after deposition of four or five cobalt monolayers onto the CoRe bilayer having a periodicity of 28 Å, but a very small lateral corrugation. It is caused by superposition of the hexagonal cobalt lattice and the Re(0001) lattice of the first bilayer, see text for more details. The three dark 'holes' in the image are due to surface defects (48 Å × 48 Å; $I_t = 0.33$ nA, $V_t = 19$ mV).

on rhenium has certainly to do with the moderately strong interaction between these two metals. Consequently, supersaturation of the two-dimensional cobalt vapor on the flat terraces is easily obtained, and nuclei form and grow homogeneously. The competing Re/Co site exchange processes, however, will additionally induce surface inhomogeneities (see below) which, in turn, can act as centers for heterogeneous nucleation. This becomes relevant at higher temperatures where we observe both with STM and LEED periodic structure elements due to reconstruction processes; for example, the formation of CoRe double rows. These in turn act as nucleation centers for further growth of cobalt islands. Quite similar phenomena have recently been reported by Brune et al. [40] who used misfit dislocation domain structures formed by silver crystallites on top of a Pt(111) surface to grow very regular silver clusters with diameters in the 30–50 Å range. Another example is the heterogeneous nucleation of nickel atoms at the elbows of the reconstructed Au(111) surface [41–43].

The interesting depletion of cobalt islands near ascending step edges can be explained by an effective trapping of the cobalt adatoms in a potential well at the downhill side of a step and a simultaneous inhibition of the transport of cobalt atoms across a step edge due to an active Schwoebel barrier [35]. This barrier repels all cobalt atoms diffusing on a higher terrace towards the descending steps and compensates for the lacking flux of adatoms from the downhill side. Accordingly, the probability for formation of homogeneous nuclei on the higher terrace near the descending step is quite comparable with that on the terrace.

### *4.2. The shape of the cobalt islands and the growth mechanism*

Depending on temperature, the geometrical shape of cobalt islands can exhibit two principally

different features. The first one is observed at 300 K and consists of fairly irregular islands with largely fringed edges of dendritic character, whereby the arms of the dendrites are definitely influenced by the three main symmetry directions of the substrate surface. The rotation of the triangular islands by 60° from terrace to terrace reflecting the preference of this hcp system to form (111) oriented microfacets (see below) was already discussed in a previous work [30]. (The other type of islands dominates at elevated temperatures and is characterized by smoother edges and an overall triangular shape, as will be dealt with further below.)

Various theoretical models have been developed to describe dendritic type of growth, among others the 'diffusion-limited aggregation' (DLA) model by Witten and Sander [44,45] which, in its simplest form, predicts totally undirected growth. The preferential growth directions observed in our experiments are due to certain anisotropies in the rate of diffusion or the condensation probability at differently oriented edges of islands. These effects are especially relevant around 300 K, where the adatom diffusion occurs preferentially along the edges of islands. Furthermore, anisotropic lattice strain can play an important role. Phenomena of this kind have been reported previously by Grütter and Dürig [46], Brune et al. [40,47], Langer [48] and Zhang et al. [49]. From our room-temperature STM data it is really apparent that a diffusing cobalt atom that hits a (111) or a (100) oriented microfacet will favor the (111) microfacet, for the STM images showed a strictly alternating orientation of the triangular cobalt islands on adjacent terraces. The reason for this interesting anisotropy is that the hcp basal plane with its A–B–A stacking sequence exhibits hcp sites (with four nearest-neighbor atoms) and fcc sites (with only three neighbors); these sites alternate for terraces with monoatomic heights as one moves upstairs or downstairs. As mentioned above, the difference in the 'easy' growth directions can then be explained by the slightly lower potential energy of the adatom in a (111) microfacet as compared with the (100) adsorption site. Very similar effects were reported by de la Figuera et al. [27] when they followed the growth of cobalt on a Cu(111) surface.

At higher temperature islands will tend to exhibit more symmetric growth forms, and the actually observed shape can reflect thermodynamic equilibrium or, in the case of still considerable diffusion activation barriers, be a result of the interplay between thermodynamics and kinetics. Usually, the growth form will be determined by the edges with the lowest activation energy for diffusion, and with the anisotropy between fcc and hcp sites given, trigonal growth forms are expected and indeed experimentally observed for $T > 400$ K. This is in full analogy to the system Ag/Pt(111) which also exhibited, at low enough temperatures, silver islands of dendritic shape [47,50].

Turning to the growth mechanism, we face the problem of how the considerable lattice misfit of $\sim 10\%$ between cobalt and rhenium can actually be overcome. The absence of a LEED superstructure for submonolayer cobalt coverages at 300 K could be interpreted (as was done with the Ag/Re(0001) system [36]) in terms of a pseudomorphic growth in the first layer, although this is hard to deduce from the few STM images of the complete first cobalt monolayer that were obtained with atomic resolution. It seems as if the cobalt atoms exhibit short-range order only (over length scales of some 50 Å) and form small crystallites which require fairly large coverages ($\Theta > 0.8$) to finally coalesce. The relatively early appearance of second-layer aggregates, along with the formation of a true epitactic LEED pattern (for $1\ \text{ML} < \Theta < 3\ \text{ML}$), suggest that an incomplete layer growth [which may be regarded as a special type of Stranski–Krastanov (SK) growth] dominates at 300 K with three-dimensional cobalt clusters of hexagonal orientation. Unfortunately, it was impossible in our experiments to probe the 'buried' interfacial region underneath the second cobalt layer to decide whether or not a pseudomorphic first cobalt layer provides relaxation of the lattice strain. What we could clearly see, however, is that the incomplete layer growth is a result of (1) the largely restricted diffusivity of cobalt atoms on both the rhenium substrate and the already existing cobalt layers, and of (2) the existence of an active Schwoebel barrier which prevents second-

(and third-) layer atoms from surmounting the edges of individual islands; at this stage, the growth of cobalt is definitely kinetically limited. We note (3) that additional atom exchange processes between the first and second layer (or better within the first ReCo bilayer) can occur along the rough edges of the cobalt islands which make it easier for cobalt atoms to leave a second-layer island and become incorporated in the first-layer film. These exchange processes will then allow a better completion of still porous monolayers, resulting in the observed incomplete layer growth instead of a genuine SK growth. Incomplete layer growth is characteristic for kinetically hindered systems <cross-ref refid="ref51"[51] and has been described also for the comparable system Ni/Ru(0001) [52]. It is very much related, if not identical, to the pseudo Frank–van der Merwe growth expected and predicted for metals which exhibit an appreciable lattice misfit and a non-negligible lattice strain energy contribution, along with a restricted mobility of the adatoms [53].

The situation changes considerably if the cobalt deposition is performed at 400 or 550 K. We saw that the cobalt edges lose their dendritic shape and become more compact; site exchange processes between rhenium and cobalt atoms are now easily possible. At a first glance one could argue that the surface free energy of the close-packed rhenium surface of 3.65 J $cm^{-2}$ [54] is far too high to allow processes of this kind. However, respective exchange phenomena were reported even for non-miscible metal-on-metal systems [53–57], specific examples being rhodium on Au(111) at 673 K [16] or rhodium on Ag(100) [15], in which the rhodium atoms could replace gold or silver atoms in the first layer. For miscible metals such as cobalt and rhenium these interchange processes should readily occur, provided the appropriate thermodynamic conditions are chosen during deposition, and indeed various studies revealed the formation of surface alloys (Ag/Pt(111) [11]; Co/Pt(111) [58]; Pb/Cu [59]). Most importantly, this holds also for the quite comparable system cobalt on Ru(0001) [60], especially at elevated temperatures.

Our 400 and 550 K STM results suggested that cobalt islands take up rhenium atoms and 'reconstruct' to a fairly homogeneous (2x2) surface alloy of stoichiometry $ReCo_2$. The uncovered rhenium surface, on the other hand, incorporates cobalt atoms to form a likewise homogeneous surface alloy of still unknown stoichiometry. Note that both surface alloys exist at the interface only and possess the lattice constant of the Re(0001) surface. We will expand on the alloy formation issue in Section 4.3.

On the alloyed bilayer genuine Co(111) crystallites grow (despite the still existing lattice misfit) and form a network of triangular misfit dislocation domains in the second and third layers, with a period length of $\sim$27 Å. Fig. 12 provides a ball model of how this structure can be rationalized. It is composed of two equilateral triangles: one made up of 66 cobalt atoms (side length = 11 atoms) with its apex pointing upwards; the other, separated from the first triangle by an empty row of threefold coordinated sites, contains 36 atoms (side length = 8 atoms). However, this model does not provide height differences between the two triangles and cannot, therefore, completely explain the STM observation (which revealed a respective height difference of 0.3 Å). Here, we can only invoke a dependence of the local charge distribution on the different stacking sequences of the

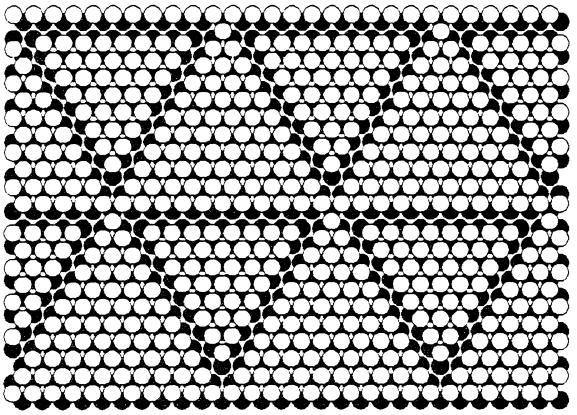

Fig. 12. Tentative real-space structure model of the network structure observed in STM after deposition of three cobalt layers at 550 K. Two kinds of equilateral triangles are separated by domain boundaries which come about by a different stacking sequence of the cobalt atoms in adjacent triangles. Note that this pure geometrical model cannot account for the observed height difference of 0.4 Å between adjacent triangular areas, which is likely due to electronic effects.

atoms in the two triangular patches which might be responsible for the slightly different imaging contrast [52,61].

We recall that cobalt coverages between three and six monolayers, deposited at 400 or 550 K, led to a pronounced Moiré pattern in the STM images (cf. Fig. 11b), with a periodicity of the unit mesh of ~27–28 Å, but almost negligible corrugation, compared with the aforementioned network of triangles. In LEED, the Moiré pattern showed up as a $(10\times10)$ structure that was not distinguishable from the $(10\times10)$ pattern of the network phase. We explain the Moiré pattern simply as a superposition of a more or less rigid stacking of genuine cobalt layers with (111) or (0001) orientation and the Re(0001) surface, without any mutual rotations of the two lattices. From a simple geometrical consideration, 11 cobalt atoms fit onto 10 rhenium atoms: $10\times2.76\ \text{Å}\approx11\times2.50\ \text{Å}$, and a tentative real-space structure model is presented in Fig. 13. Support for this interpretation comes from

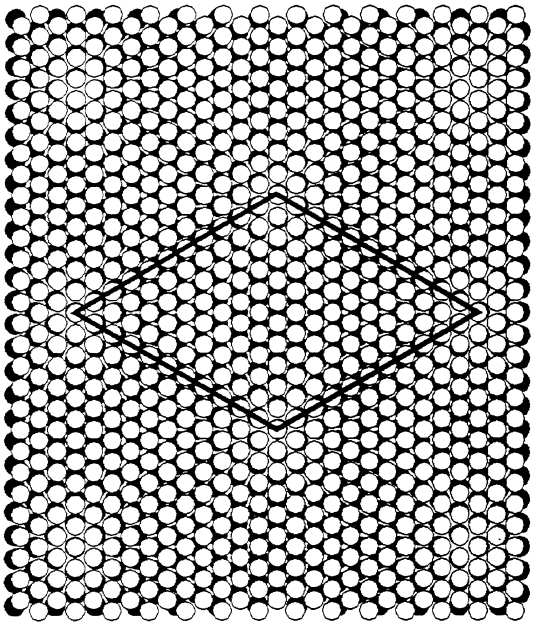

Fig. 13. Real-space structure model of the Moiré pattern formed by stacking of a hexagonal cobalt layer (with its characteristic lattice parameters) on top of a hexagonal surface with the rhenium lattice parameter. No rotation of the two lattices with respect to each other is required to account for the observed periodicity of ~28 Å. See text for more details.

LEED experiments which reveal that the fractional-order beams of the $(10\times10)$ pattern are centered around the Co(111) spots and not around the Re(0001) reflexes. Furthermore, the $(2\times2)$ spots are no longer visible. A detailed description and interpretation and of these phenomena will be provided in a forthcoming publication [62].

### *4.3. The formation of CoRe surface alloys at the interface*

#### *4.3.1. The 'vacancy' phase at 400 K*

A particularly interesting observation of our work is the formation of the $(2\times2)$ 'vacancy' phase repeatedly mentioned above. This phase is induced by cobalt atoms on the bare Re(0001) surface and can be seen even at 300 K, but dominates the surface morphology at 400 and 550 K. At first glance, the observed STM imaging depth of ~1 Å would suggest the presence of real *vacancies* in the surface, with the requirement that rhenium atoms must have been *removed* from their original lattice positions quite regularly and transported to a different location. This removal would, however, be physically highly unlikely for energetic reasons: a Re$(2\times2)$ vacancy phase would exhibit an extremely large surface tension, making this surface structure entirely unstable. Another, much more realistic, possibility is that the dark 'holes' actually represent atoms which are *invisible* with STM due to a peculiar chemical contrast. The incorporated atoms help to stabilize the $(2\times2)$ surface phase. Since we can clearly rule out impurity atoms (there are no indications for carbon or sulfur nor any other contaminants) we correlate the appearance of the $(2\times2)$ 'vacancy' phase [which exhibits the periodicity of the Re(0001) surface] with the presence of *cobalt atoms* on and in the rhenium surface. A strong chemical contrast has been confirmed especially for cobalt atoms alloyed with platinum metals [20,21], in which the platinum atoms always represented the 'brighter' and cobalt the 'darker' species. The fact that the 'vacancies' are predominantly formed *near cobalt islands* and spread from these islands across the entire rhenium surface suggest that a surface exchange process must have taken place in which cobalt atoms have replaced every second rhenium

atom. If our interpretation of the vacancy phase is correct then every rhenium atom is surrounded by three (invisible) cobalt atoms, and one could deduce a stoichiometry of $ReCo_3$ for this surface alloy phase. However, the different depth profiles of the vacancies possibly suggest a more complicated surface composition. The 'invisible' atoms could probably be detected by additional ion-scattering experiments or by quantitative LEED ($I$–$V$) measurements of the $(2\times2)$ fractional-order spots (measurements of this kind are planned for the future).

The determination of structure and morphology of the $(2\times2)$ phases including their chemical composition is essential for a further elucidation of the underlying interdiffusion and alloy formation mechanism(s). This implies the interesting mystery of how the necessary transport of the periodically displaced rhenium atoms proceeds. It appears from our STM images (especially from those taken from the 550 K films) that the presence of a few cobalt atoms only already makes the whole rhenium surface unstable, because a large number of (mostly single) vacancies is formed only once the rhenium surface has been exposed to cobalt vapor. For a more extensive treatment of these issues we refer to our forthcoming paper [62].

*4.3.2. Surface alloys at 550 K*

At elevated temperatures the situation is entirely different. $(2\times2)$-Structured Co–Re surface alloys of different stoichiometry are formed right at the interface and provide enough relaxation so that genuine cobalt layers can grow even in the third, fourth or fifth layer. We recall that these alloys were formed either after direct deposition at elevated temperatures, or after annealing of room-temperature deposits to 550 K. The fact that mere annealing causes the formation of a periodic phase is rather unusual. Unreactive bimetallic systems, e.g., silver on Re(0001) [36], do not tend to improve their lateral ordering noticeably upon annealing of coldly deposited layers. The peculiar behavior of the Co/Re(0001) system suggests that the aforementioned development of the $(2\times2)$ or $(10\times10)$ phase is not simply a mere ordering phenomenon of a formerly disordered layer, but rather reflects an irreversible, thermally activated, reactive phase transformation which involves the formation of an ordered phase right at the Re/Co interface. We know already from room-temperature STM experiments and the respective images taken from the 400 K films that the ordered $(2\times2)$ phase consists of CoRe surface alloys with various stoichiometries, the most favored one being $ReCo_3$. We emphasize again that the formation of these alloys is limited to the direct interface, we never obtained evidence that rhenium atoms could penetrate even a two-monolayer cobalt film and appear at the surface; rather, genuine cobalt islands grow on top of the Re–Co bilayer at the interface. On the other hand, thermal desorption experiments performed with cobalt layers on Re(0001) showed that the cobalt could be practically entirely removed from the rhenium surface which underlines the observation that no CoRe bulk alloys (which do exist [22]) are formed under our experimental conditions.

In summary, it has been shown that Co/Re is a highly reactive system at elevated temperatures which exhibits strongly corrosive surface/interface diffusion processes leading to a variety of Co/Re surface alloys.

## Acknowledgements

The authors gratefully acknowledge fruitful discussions with D. Schlatterbeck and technical help from R. Cames and K. Schubert. This work would not have been possible without financial support from the Deutsche Forschungsgemeinschaft through SFB 290.

## References

[1] P. Wissmann (Ed.), Studies in Surface Science and Catalysis 32 Elsevier, Amsterdam, 1987.
[2] B.T. Jonker, J.P. Hereman, E.E. Marinero, Growth, Characterization and Properties of Ultrathin Magnetic Films and Multilayers, Materials Research Society, Pittsburgh, PA, 1989.
[3] R.J. Behm, W. Hosler, in: R. Vanselow Howe (Eds.), Chemistry and Physics of Solid Surfaces VI, Springer-Verlag, Berlin–New York, 1986, p. 361. (Chapter 14).
[4] J. Wintterlin, R.J. Behm, in: H.J. Güntherodt, R. Wiesen-

danger (Eds.), Scanning Tunneling Microscopy, 2nd. ed. I Springer-Verlag, Berlin–Heidelberg–New York, 1994.
[5] J.H. Van der Merwe, in: R. Vanselow Howe (Eds.), Chemistry and Physics of Solid Surfaces V Springer-Verlag, Berlin–New York, 1984 (Chapter 16).
[6] J.A. Venables, Surf. Sci. 299/300 (1994) 798.
[7] D.J. Smith, in: R. Vanselow Howe (Eds.), Chemistry and Physics of Solid Surfaces VI Springer-Verlag, Berlin–New York, 1986.
[8] P. Ruggerone, C. Ratsch, M. Scheffler, in: D.A. King, D.P. Woodruff (Eds.), The Chemical Physics of Solid Surfaces 8 Elsevier Science, New York, 1997.
[9] H. Brune, Surf. Sci. Rep. 31 (1998) 121.
[10] P. Hu, A. Wander, L. Morales de la Garza, M.P. Bessent, D.A. King, Surf. Sci. 286 (1993) L542.
[11] D.A. Hutt, D.W. Bassett, Surf. Sci. 287/288 (1993) 1000.
[12] U. Bardi, Rep. Progr. Phys. 57 (1994) 939.
[13] P.T. Wouda, B.E. Nieuwenhuys, M. Schmid, P. Varga, Surf. Sci. 359 (1996) 17.
[14] S. Robert, S. Gauthier, F. Bocquet, S. Rousset, J.L. Duvalt, J. Klein, Surf. Sci. 358 (1996) 136.
[15] S.L. Chang, J.–M. Wen, P.A. Thiel, S. Günther, J.A. Meyer, R.J. Behm, Phys. Rev. B 53 (1996) 13747.
[16] E.I. Altman, J.R. Colton, Surf. Sci. Lett. 304 (1994) L400.
[17] G. Gilarowski, H. Niehus, in press.
[18] H.P. Oepen, A. Berger, C.M. Schneider, T. Reul, J. Kirschner, J. Magnetism Magn. Mater. 121 (1993) 490.
[19] A. Brodde, K. Dreps, J. Binder, Ch. Lunau, H. Neddermeyer, Phys. Rev. B 47 (1993) 6609.
[20] P. Varga, plenary lecture given at the Spring Meeting of the German Physical Society, Münster/Westf., 1997.
[21] Y. Gauthier, P. Dolle, R. Baudoing-Savois, W. Hebenstreit, E. Platzgummer, M. Schmid, P. Varga, Surf. Sci. 396 (1998) 137.
[22] W. Köster, E. Horn, Z. Metallkunde 43 (1952) 444.
[23] C.T. Campbell, Annu. Rev. Phys. Chem. 41 (1990) 775.
[24] J.A. Rodriguez, Surf. Sci. Rep. 24 (1996) 224.
[25] R.Q. Hwang, C. Günther, J. Schröder, S. Günther, E. Kopatzki, R.J. Behm, J. Vac. Sci. Technol. A 10 (1992) 1970.
[26] M. Stindtmann, M. Farle, T.S. Rahman, L. Benabid, K. Baberschke, Surf. Sci. 381 (1997) 12.
[27] J. de la Figuera, J.E. Prieto, C. Ocal, R. Miranda, Phys. Rev. B 47 (1993) 13043.
[28] H. Li, B.P. Tonner, Surf. Sci. 237 (1990) 141.
[29] M. Wuttig, B. Feldmann, T. Flores, Surf. Sci. 331–333 (1995) 659.
[30] M. Parschau, K. Christmann, Ber. Bunsenges. Phys. Chem. 99 (1995) 1376.
[31] D. Schlatterbeck, M. Parschau, K. Christmann, in preparation.
[32] D'Ans-Lax, Taschenbuch für Chemiker und Physiker, 3rd ed. Springer-Verlag, Berlin–Heidelberg–New York, 1967.
[33] T. Michely, M. Hohage, M. Bott, G. Comsa, Phys. Rev. Lett. 70 (1993) 3943.
[34] J. Jacobsen, K.W. Jacobsen, J.K. Nørskov, Surf. Sci. 359 (1996) 37.
[35] R.L. Schwoebel, J. Appl. Phys. 40 (1969) 614.
[36] M. Parschau, D. Schlatterbeck, K. Christmann, Surf. Sci. 376 (1997) 133.
[37] C. Günther, S. Günther, E. Kopatzki, R.Q. Hwang, J. Schröder, J. Vrijmoeth, R.J. Behm, Ber. Bunsenges. Phys. Chem. 97 (1993) 522.
[38] E. Kopatzki, S. Günther, W. Nichtl-Pecher, R.J. Behm, Surf. Sci. 284 (1993) 154.
[39] C.L. Liu, M.J. Cohen, J.B. Adams, A.F. Voter, Surf. Sci. 253 (1991) 334.
[40] H. Brune, H. Röder, C. Boragno, K. Kern, Phys. Rev. B 49 (1994) 2997.
[41] D.D. Chambliss, R.J. Wilson, S. Chiang, J. Vac. Sci. Technol. A 10 (1992) 1993.
[42] D.D. Chambliss, R.J. Wilson, S. Chiang, Phys. Rev. Lett. 66 (1991) 1721.
[43] J.A. Meyer, I.D. Baikie, E. Kopatzki, R.J. Behm, Surf. Sci. 365 (1996) L647.
[44] T.A. Witten, L.M. Sander, Phys. Rev. Lett. 47 (1981) 1400.
[45] T.A. Witten, L.M. Sander, Phys. Rev. B 27 (1983) 5686.
[46] P. Grütter, U.T. Dürig, Surf. Sci. 337 (1995) 147.
[47] H. Brune, K. Bromann, H. Röder, K. Kern, Nature 369 (1994) 469.
[48] J.S. Langer, Science 243 (1989) 1150.
[49] Z. Zhang, X. Chen, M.G. Lagally, Phys. Rev. Lett. 73 (1994) 1829.
[50] H. Röder, K. Bromann, H. Brune, K. Kern, Phys. Rev. Lett. 74 (1995) 3217.
[51] J. Vrijmoeth, C. Günther, J. Schröder, R.Q. Hwang, R.J. Behm, in: R.F.C. Farrow et al. (Eds.), Magnetism and Structure in Systems of Reduced Dimension, Plenum Press, New York, 1993, p. 55.
[52] J.A. Meyer, P. Schmid, R.J. Behm, Phys. Rev. Lett. 74 (1995) 3864.
[53] E. Bauer, Ber. Bunsenges. Phys. Chem. 95 (1991) 1315.
[54] A. Miedema, J. Dorleijn, Surf. Sci. 95 (1990) 447.
[55] L.P. Nielsen, F. Besenbacher, I. Stensgaard, E. Laegsgaard, C. Engdahl, P. Stoltze, K. Jacobsen, J.K. Norskøv, Phys. Rev. Lett. 71 (1993) 754.
[56] H. Röder, R. Schuster, H. Brune, K. Kern, Phys. Rev. Lett. 71 (1993) 2086.
[57] J.L. Stevens, R.Q. Hwang, Phys. Rev. Lett. 74 (1995) 2078.
[58] A. Atrei, U. Bardi, M. Galeotti, G. Rovida, M. Marco, R. Zanazzi, Surf. Sci. 339 (1995) 323.
[59] C. Nagl, E. Platzgummer, O. Haller, M. Schmid, P. Varga, Surf. Sci. 331–333 (1995) 831.
[60] R.Q. Hwang, Phys. Rev. Lett. 76 (1996) 4757.
[61] C. Günther, J. Vrijmoeth, R.Q. Hwang, R.J. Behm, Phys. Rev. Lett. 74 (1995) 754.
[62] D. Schlatterbeck, M. Parschau, K. Christmann, in preparation.